CEBAF-PR-95-028

Strategies for minimizing emittance growths in high intensity CW FEL injectors

H. Liu

CEBAF, 12000 Jefferson Avenue, Newport News, VA 23606, USA

Corresponding author:

Hongxiu Liu MS 12 A1
Continuous Electron Beam Accelerator Facility
Newport News, VA 23606 USA
Phone: (804) 249 - 6381
Fax: (804) 249 - 5024
E-mail: LIU@cebaf.gov

Abstract

We discuss beam emittance growths in high intensity CW FEL injectors due to linear and non-linear space charge fields, phase space bifurcation, skew-quad effect, longitudinal momentum modification by space charges in bends, and equipartitioning, etc. We generalize Kim's RF laser gun theory to DC laser guns. We discuss the traditional free energy theory of emittance growth. The best strategies for designing high-intensity CW FEL injectors are derived, and their application to the design analysis of the CEBAF 10 MeV DC laser gun CW FEL injector test stand is discussed.

1. Introduction

A DC photoemission gun [1,2] is being built at CEBAF as part of a 10 MeV CW high-intensity FEL injector [3]. This injector should provide high-brightness e-beams for a two-pass 200 MeV SRF driver accelerator [4] for a kW UV FEL being designed at CEBAF [5]. The design has been iterated over a few years [6-10], and finalized recently [3, 11], with the requirements shown in Table 1 satisfied. In this paper, we discuss the best strategies for circumventing emittance growths in high-intensity CW FEL injectors.

2. Emittance growth mechanisms

2.1 Emittance growth in a DC laser gun

Kim's theory [12] has been widely used for RF laser guns. We generalize it to a DC laser gun by ignoring the RF effect which does not exist in a DC laser gun as follows

$$\varepsilon_{nirms}^{sc\,(linear)} = 30 arccos\,(1/\gamma_f)\,(I/E_0)\,\mu_i(A),\ \ (i = x, z)\ (\pi\ mm\ mrad) \qquad (1)$$

where γ_f is the beam energy at the gun exit, $I = Q/\sqrt{2\pi}\sigma_t$ the peak current in A, E_0 the DC field gradient at the cathode in MV/m, $A=\sigma_x/\sigma_z$ the aspect ratio of the beam at the gun exit, and $\mu_x^{-1}(A) = 3A + 5$, $\mu_z^{-1}(A) = 1 + 4.5A + 2.9A^2$ for Gaussian distributions. In Eq. (1), we use "*linear*" to emphasize that it belongs to the category of the linear space charge effect, namely, slice-to-slice effect. This sort of emittance growth can be compensated using a solenoid [13].

The free energy theory [14] says that when initial beam distributions are nonuniform, the

excess energy carried with the beam will be converted into thermal energy or emittance through a rapid charge redistribution process (in one quarter plasma period) driven by nonlinear space charge fields. It provides a unique criterion for estimating the optimization level of a design with emittance growth control as one of the major goals. According to free energy theory [14]

$$\varepsilon_{nxrms}^{(f)} = \sqrt{\left(\varepsilon_{nxrms}^{(i)}\right)^2 + \frac{Nr_c\sigma_x}{15\sqrt{5}\gamma_0}\frac{U}{W_1}}, \qquad (2)$$

where N is the number of electrons in a bunch, r_c=2.82×10^{-15} m, σ_x the transverse rms size of the beam, γ_0 the relativistic energy factor, and U/W_1 the normalized free energy equal to 0.308 for a Gaussian distribution and 0.0368 for a parabolic distribution. Assuming that the initial emittance is small then we arrive at a surprising result

$$\varepsilon_{nxrms}^{(f)} = \sqrt{\frac{Nr_c}{15\sqrt{5}\gamma_0}\frac{U}{W_1}\sigma_x}, \qquad (3)$$

which indicates that the final emittance is determined by both the initial beam distributions and the initial beam size. It provides guidelines for minimizing the asympototic or final emittance.

It is interesting to note from Eqs. (1) and (3) that if the emittance is dominated by the linear space charge effect then the final emittance is proportional to the peak current (Kim's theory), and that if the emittance growth is dominated by the non-linear space charge effect, then the final emittance is proportional to the square root of charge/bunch (free energy theory). By looking at the dependence of the final emittance on the peak current and charge/bunch, one can determine

whether the emittance growth is dominated by the linear or nonlinear space charge effect.

2.2 Emittance growth during beam focussing and compression

When the electrons are focussed and compressed, transverse and axial crossovers may occur. At a crossover, close-range Coulomb interaction among electrons may result in phase space mixing and loss of coherence in their behavior in the form of phase space bifurcation or growth of effective emittance. Bifurcation phenomenon in the transverse phase space was first reported by Hanerfeld et al. [15], and was encountered in the Los Alamos FEL injector simulations as well [16]. In our injector design, bifurcations have shown up in both the transverse and longitudinal phase spaces [10]. This phenomenon is not yet described analytically.

2.3 Emittance growth due to skew quad effect

Skew quad effect originates from the asymmetry of an accelerator structure. It can be minimized by minimizing the beam size at the entrance of the accelerating section, or compensated by using a skew quad before the accelerating section [17]. However, the compensation is incomplete in the presence of space charge. This effect is important in the first few cavities of the driver accelerator as well.

2.4 Emittance growth in a beam injection line

A bending system (horizontal) introduces x-z correlation to the electrons, resulting in a large growth of effective emittance at the symmetry plane

$$\Delta\varepsilon_{nxrms} = (\eta_c / f_x)\,\sigma_{\gamma\beta}(0)\,\sigma_x(0), \qquad (4)$$

where η_c is the maximum dispersion at the symmetry plane, f_x the focal length of the first half of the system, $\sigma_{\gamma\beta}(0)$ the initial rms momentum spread which can be large when beam compression is desired through the bending system, and $\sigma_x(0)$ the initial rms beam size in the x-plane. This sort of emittance growth is removed completely in an achromatic bending system. However, space charge may deteriorate the achromaticity by modifying the energy of the electrons, resulting in an incomplete cancellation of the x-z correlation and a residual emittance growth [18,19]. It's desirable to minimize the dispersion, beam momentum spread and beam size in order to ease the emittance cancellation through the achromaticity of the system.

2.5 Emittance growth due to equipartitioning

Equipartitioning [14] is related to temperature balancing in the transverse and longitudinal dimensions. This concept is valid only when the velocity distributions are of the Maxwell-Boltzmann-type, and when the beam's motion obeys the smooth approximation [20]. Launching a non-equilibrium beam leads to fast reorganization of the populated phase space towards a self-consistent phase space density function in two different fashions [21]: (1) the charge density in a non-self-consistent state will redistribute; this leads to a rapid emittance growth in a quarter plasma period, which is independent of whether the beam temperatures are balanced or not; (2) the temperatures in x, y and z will balance, but the time scale for the related redistribution process is significantly larger (in most cases about 10 plasma periods). Equipartitioning generally is not an issue in an electron injector due to its long relaxation time.

3. Strategies

Some strategies are fairly straightforward and well-known. A high external field gradient at the cathode is always beneficial to suppressing the initial rapid emittance growth; the beam distributions in various dimensions should be as uniform as possible; the entire system should be compact. There are limitations to these approaches in practice. Here we restrict our discussion on the best design strategies to those resulting from beam dynamics.

Such strategies include: (1) utilizing a small emission area; by doing so, one can minimize the initial emittance and hence the final emittance from the free energy point of view; one can also maximize the ratio of the linear space charge field induced emittance to the thermal emittance, and therefore make the most of an emittance compensating solenoid; (2) one should minimize the number of crossovers along the system to avoid phase space bifurcation and to help reduce system sensitivity; (3) the beam transport injection line should have smallest possible dispersion at the symmetry plane.

4. Application

We were most interested in a high-degree of optimization in our FEL injector design for the best emittance performance with a given set of hardware constraints. A package of widely used computer codes, POISSON(gun and solenoids), SUPERFISH(buncher), and MAFIA(SRF cavities) was used with the skeleton beam dynamics code PARMELA in optimizing our injector design. The space charge effects were included through the entire system from the cathode to the

driver accelerator using a point-by-point space charge algorithm [22, 23] benchmarked [24] against ISIS [25]. Good agreement has been recently achieved between modeling with this algorithm and experiment on the CEBAF 5-pass 4-GeV superconducting accelerator injector.

The optimized system performance, using the strategies discussed above, is shown in Fig. 1, with the transverse and longitudinal beam envelopes shown in Fig. 2. The following initial beam parameters at the cathode were used: charge/bunch 135 pC, gun voltage 500 kV, DC field gradient E_0 = 10 MV/m, beam pulse length 90 ps ($6\sigma_t$); the thermal energy distribution of the electrons was assumed to be Gaussian with a mean kinetic energy of 0.3 eV and an rms energy spread of 0.1 eV. We found that a small laser spot size of 2 mm (diameter, $4\sigma_x$) at the cathode is optimal for the smallest emittance at the end of the injector.

The injection line design has a high degree of beam quality preservation and was discussed in detail in Ref. [19]. Here we discuss the straight-line part of the design from the gun to the entrance of the first dipole where Kim's theory and free energy theory apply. We first estimate the emittance growth using Kim's theory. At the gun exit, σ_x/σ_z=0.3, I=3.6 A, γ_f=2, we obtain ε_{nxrms}=1.9 π mm mrad and ε_{nzrms}=4.8 π deg-keV, both of which are smaller than that of 2.3 π mm mrad and 6.6 π deg-keV from the simulation (see Fig. 1). The differences can be explained by noting that in Kim's theory only linear space charge effect is included, whereas in simulation both linear and nonlinear space charge effects were included. This explanation is supported by the distorted longitudinal phase space distribution due to nonlinear space charge fields, as shown in Fig. 3.

Kim's theory does not predict the asymptotic emittance, since charge redistribution and compensation effect from a solenoid are not taken into account. This is where the traditional free energy theory of emittance has its greatest efficacy. Using Eq. (3) with N=8.4×10^8, $\sigma_x(0)$=0.5 mm, $\varepsilon_{nxrms}^{(i)}$=0.5 π mm mrad and U/W_1=0.308, we obtain $\varepsilon_{nxrms}^{(f)}$ =3.3 π mm mrad, which agrees surprisingly with that of 3.5 π mm mrad from the simulation shown in Fig. 1 at the entrance of the first dipole of the injection bending system. This excellent agreement indicates that free energy injected by the beamline components is minimal, and the design strategy successfully keeps the emittance from growing significantly.

In Fig. 4, we show beam distributions at the exit of the cryounit and entrance to the driver accelerator. Although we have made the beam collimated in several regions of the system, bifurcations occurred in both transverse and longitudinal phase spaces due to focussing and bunching prior to the cryounit. The bifurcated particles turn into a halo around the core of the beam, as shown in Fig. 4 (h), and may get lost in the transport line. This issue is under further investigation.

Acknowledgments

I thank S. Benson, J. Bisognano, C. Bohn, F. Dylla, D. Engwall, D. Kehne, G. Neil, D. Neuffer and C. Sinclair for discussions. I wish to thank B. Carlsten, M. Reiser, T. Raubenheimer, and J. Struckmeier for discussions about some of the topics in this paper. This work was supported by the Virginia Center for Innovative Technology and DOE Contract # DE-AC05-84ER40150.

References

[1] C. Sinclair, *Nucl. Instrum. Methods* **A 318** (1992) 410.

[2] L. Cardman and D. Engwall, private communication.

[3] H. Liu et al., *Proc. of 1995 Particle Accelerator Conf.*, Dallas TX (1995).

[4] D. Neuffer et al., these proceedings.

[5] F. Dylla et al., *Proc. of 1995 Particle Accelerator Conf.*, Dallas TX (1995).

[6] P. Liger et al., *Nucl. Instrum. Methods* **A 318** (1992) 290.

[7] P. Liger et al., *1992 Linear Accelerator Conference Proceedings* (AECL-10728) 85.

[8] H. Liu et al., *Proc. 1993 Particle Accelerator Conf.*, p. 3663.

[9] H. Liu et al., *Nucl. Instrum. Methods* **A339** (1994) 415.

[10] H. Liu et al., *Nucl. Instrum. Methods* **A358** (1995) 475.

[11] Chap. 4, *CEBAF FEL Conceptual Design Report*, 1995, unpublished.

[12] K. Kim, *Nucl. Instrum. Methods* **A275** (1989) 201.

[13] B. Carlsten, *Nucl. Instrum. Methods* **A 285** (1989) 313.

[14] M. Reiser, *Theory and Design of Charged Particle Beams,* (John Wiley & Sons, Inc., New York), 1994.

[15] H. Hanerfeld, W. Herrmannsfeldt and R. H. Miller, SLAC-PUB-4916 (1989).

[16] B. Carlsten, private communication.

[17] Z. Li, Ph. D. Disertation, College of William and Mary, 1995.

[18] B. Carlsten and T. Raubenheimer, *Phys. Rev.* E **51** (1995), 1453.

[19] H. Liu and D. Neuffer, *Proc. of 1995 Particle Accelerator Conf.*, Dallas TX (1995).

[20] M. Reiser, private communication.

[21] J. Struckmeier, private communication.

[22] K. McDonald, *IEEE Trans. Electron Devices* **ED-35** (1988) 2052.

[23] H. Liu, *Computational Accelerator Physics,* AIP Conf. Proc. No. 297 (1994).

[24] H. Liu, CEBAF TN# 94-040.

[25] M. Jones and B. Carlsten, *Proc. 1987 IEEE Particle Accelerator Conf.*, p.1319.

Table 1 Requirements on the CEBAF CW FEL injector

Beam parameters	Requirements
Momentum (p)	10 MeV/c
Charge/bunch (Q)	135 pC
Repetition rate (f_p)	37.43 MHz
Tran. norm. emittance (ε_{nrms})	8 π mm mrad
Longitudinal emittance ($\varepsilon_{\phi rms}$)	20 π keV-deg
Bunch length (σ_t)	1.5 ps
Matching conditions (β_x/β_y, α_x/α_y)	30/30 m, 0/0

Figure Captions

Fig. 1 Beam property evolution in the nominal design of the CEBAF FEL injector. The components in sequence are: a 500 kV DC laser gun, a solenoid, a single-cell 1497 MHz RF buncher, another solenoid, a cryounit containing two CEBAF SRF cavities, and an injection line consisting of a 4-quad zoom lens and a 3-dipole bending system with a net bending angle of 20°.

Fig. 2 Transverse and longitudinal beam envelopes along the system.

Fig. 3 Beam distributions at the exit of the gun.

Fig. 4 Phase space distributions: (a) - (d) at the exit of the cryounit; (e) - (h) at the entrance to the driver accelerator. Note halo formation in transverse velocity distribution.

Hongxiu Liu Fig. 1

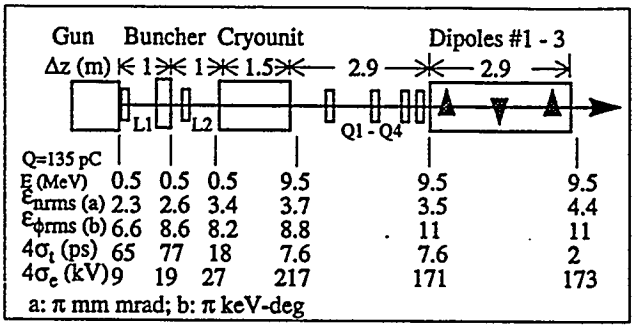

Hongxiu Liu

Fig. 2

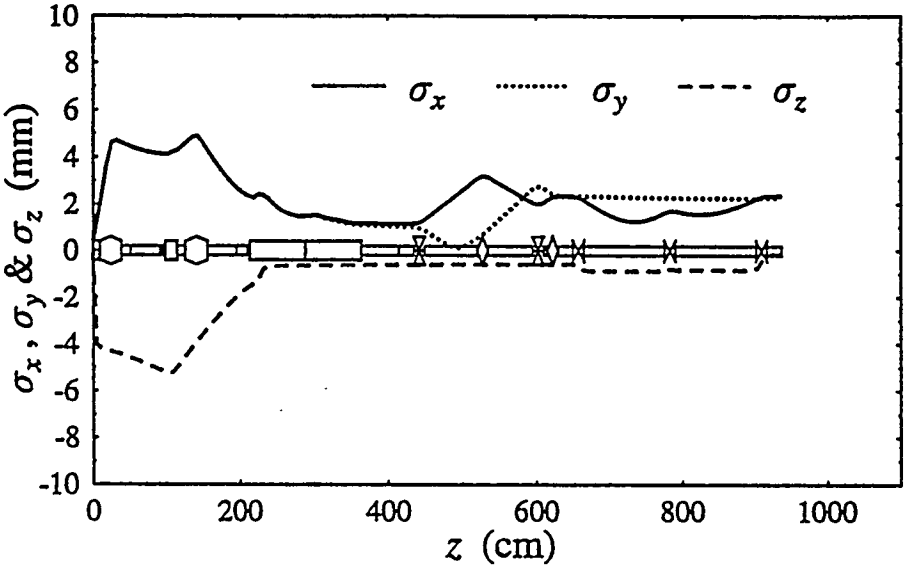

Hongxiu Liu
Fig. 3

CEBAF UV FEL INJECTOR MODELING (Exit # 1; N_{good} = 8000)

E_{beam} = .502 MeV ; $4\sigma_\phi$ = 34.9 deg. ; $4\sigma_E$ = 8.72 keV ; ϵ_z = 6.56 pi deg-keV; f_{56} = .764 m
ϵ_{nxrms} = 2.27 pi mm mrad ; σ_x = 1.9636 mm ; σ_{xp} = 18.6 mrad ; β_x = 2.91 m ; α_x = -27.5
ϵ_{nyrms} = 2.25 pi mm mrad ; σ_y = 1.9634 mm ; σ_{yp} = 18.6 mrad ; β_y = 2.93 m ; α_y = -27.7

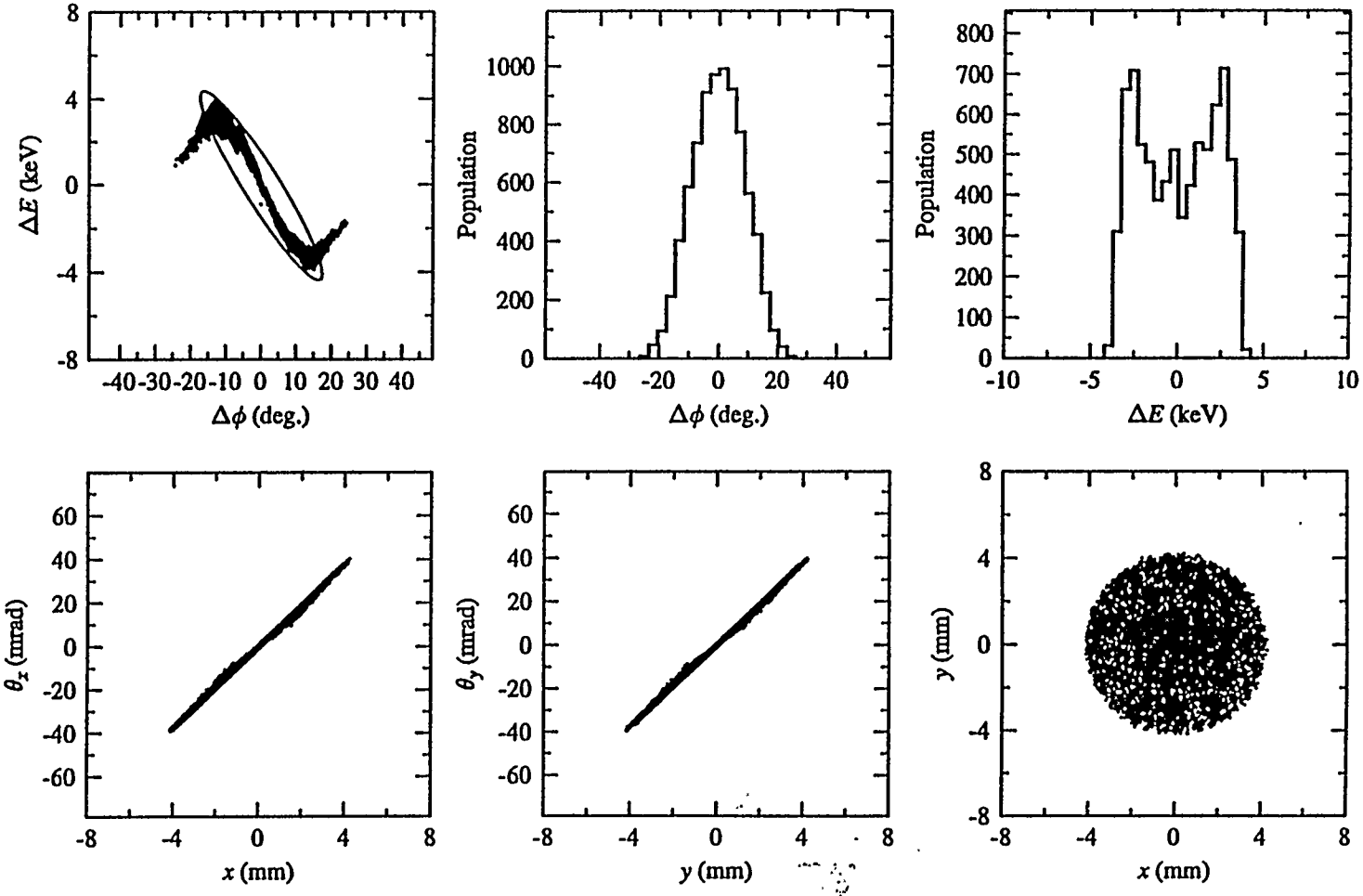

Hongxiu Liu
Fig. 4